An N-atom Collective State Atomic Interferometer with Ultra-High Compton Frequency and Ultra-Short de Broglie Wavelength, with root-N Reduction in Fringe Width

Supplementary Material

Resham Sarkar,[1,*] May E. Kim,[1] Renpeng Fang,[1] and Selim M. Shahriar[1,2]

[1] *Department of Physics and Astronomy, Northwestern University, 2145 Sheridan Road, Evanston, IL 60208, USA*

[2] *Department of Electrical Engineering and Computer Science, Northwestern University, 2145 Sheridan Road, Evanston, IL 60208, USA*

(Dated: December 16, 2014)

I. PHYSICAL INTERPRETATION OF FRINGE NARROWING

As shown in the main body of the paper, the signal of a Collective State Atomic Interferometer (CSAI), which is a measure of the probability of finding all the atoms of the ensemble simultaneously in state $|g\rangle$, narrows with the increase in the number of atoms in the ensemble. Here, we illustrate the physical mechanism that leads to this narrowing. To start with, we revisit first the physical phenomena governing the signal fringe in a Conventional Raman Atomic Interferometer (CRAI). As noted in the main body of the paper, in the application of a CRAI as a gyroscope, $\Delta\phi$ is the measure of its rotation sensitivity, arising due to the Sagnac effect [1]. The phase shift induced due to rotation along an axis perpendicular to it with at a rate of Ω_G is then $\Delta\phi = 2\Theta m\Omega_G/\hbar$, where Θ is the area enclosed by the trajectories taken by the atomic states. This expression can be derived by two different methods. The equivalence of these approaches can be seen [2–5] by noting how the de Broglie wavelength for a moving particle arises naturally from the rest frame Compton frequency via Lorentz transformation. Without loss of generality, let us consider the direction of the velocity of the particle as $\hat{\mathbf{x}}$. For non-relativistic velocities, mixing between the spinors can be ignored, and the phase factor of a positive energy spinor, in the rest

* rsarkar@u.northwestern.edu

frame of the particle, is given simply as $\exp(-i\phi)$, where $\phi = \omega_C \tau$ with τ being the proper time. The phase, ϕ, is a Lorentz invariant parameter, and can in general be written as a contraction between the position four vector x^μ and momentum four vector $\hbar k^\mu : \phi = k_\mu x^\mu$. In the rest frame of the particle, the position four-vector is $x^\mu = \{c\tau, 0, 0, 0\}$ and the momentum four vector is $\hbar k^\mu = \hbar\{\omega_C/c, 0, 0, 0\}$. In the laboratory frame, the position four vector is, by definition, $x^\mu = \{ct, 0, 0, 0\}$, and application of Lorentz transform shows that the momentum four vector is $\hbar k^\mu = \hbar\{\omega'_C/c, k_{dB}, 0, 0\}$, where $k_{dB} = \gamma m V/\hbar = 2\pi/\lambda_{dB}$ and the phase factor becomes $\phi = \omega'_C t - k_{dB} x$. Again, in the non-relativistic limit, $\gamma \approx 1$ and we get $\lambda_{dB} \approx 2\pi\hbar/mV$. Thus, the de Broglie wavelength is simply the laboratory frame manifestation of the phase variation in the rest frame due to the Compton frequency.

As discussed in the main body, we treat the Raman atomic excitation as an effective two level transition excited by a single frequency optical field. To illustrate the Sagnac effect in a CRAI in a generalized way where the role of the Compton frequency becomes more transparent, we consider the product state of the atom and a Fock state with N' photons denoted by $|N'\rangle$ or with $N'-1$ photons denoted by $|N'-1\rangle$. Thus, at $t = 0$, the atom photon system is assumed to be in the state $|g\rangle\,|N'\rangle \equiv |g, N'\rangle$. The atom-field interaction couples it to the state $|e\rangle\,|N'-1\rangle \equiv |e, N'-1\rangle$, as illustrated in 1(a). We assume that the photon energy, $\hbar\omega$, exactly matches the energy difference between the atomic internal states $|e\rangle$ and $|g\rangle$. We define the dressed frequency of the atom-photon system as ω_{PA}, which is a constant, for all possible states of the system. If we define $\omega_{C,e} = m_e c^2/\hbar$ as the Compton frequency of the excited atom, where $m_e = m_g + \hbar\omega/c^2$ is the rest mass of the excited atom, and $m_g = m$ is the rest mass of the atom in the ground state, then we have $\omega_{PA} = m_e c^2/\hbar + (N'-1)\omega = m_g c^2/\hbar + N'\omega$. The Compton frequency of the atom in the ground state is $\omega_{C,g} = m_g c^2/\hbar$. The effect of temporal phase accumulation on the system during an interval Δt, if the system is in an arbitrary superposition of $|g\rangle$ and $|e\rangle$, i.e. $c_g\,|g\rangle + c_e\,|e\rangle$ at the start of the interval, will be $\exp(-i\omega_{PA}\Delta t)(c_g\,|g, N'\rangle + c_e\,|e, N'-1\rangle)$. Thus, after the first $\pi/2$ pulse of a time duration, τ, the quantum state of the system is $\exp(\omega_{PA}\tau)(|g, N'\rangle_A - i\,|e, N'-1\rangle_B)/\sqrt{2}$, where the subscripts A and B indicate the lower and upper trajectory of the interferometer, respectively. This is followed by a dark zone of duration T_d at the end of which the quantum state of the system is $\exp(-i\omega_{PA}(\tau + T_d))(|g, N'\rangle_A - i\,|e, N'-1\rangle_B)/\sqrt{2}$. A π-pulse is applied at the end of the first dark zone, and therefore, at $t = 3\tau + T_d$, the quantum state of the system

is $|\psi(3\tau+T_d)\rangle = |\psi(3\tau+T_d)\rangle_A + |\psi(3\tau+T_d)\rangle_B$, where $|\psi(3\tau+T_d)\rangle_A = -i\exp(-i\omega_{PA}(3\tau+T_d))\,|e,N'-1\rangle/\sqrt{2}$ and $|\psi(3\tau+T_d)\rangle_B = -\exp(-i\omega_{PA}(3\tau+T_d))\,|g,N'\rangle/\sqrt{2}$. At this point the second dark zone begins, at the end of which the state of the system can be written as $|\psi(3\tau+2T_d)\rangle = |\psi(3\tau+2T_d)\rangle_A + |\psi(3\tau+2T_d)\rangle_B$, where $|\psi(3\tau+2T_d)\rangle_A = -i\exp(-i\omega_{PA}(3\tau+2T_d))\,|e,N'-1\rangle/\sqrt{2}$ and $|\psi(3\tau+2T_d)\rangle_B = -\exp(-i\omega_{PA}(3\tau+2T_d))\,|g,N'\rangle/\sqrt{2}$. Finally, the last $\pi/2$-pulse causes each of the arms to further split in to $|g,N'\rangle$ and $|e,N'-1\rangle$, so that the state of the system at $t = 4\tau+2T_d$ is given by $|\psi(4\tau+2T_d)\rangle = |\psi(4\tau+2T_d)\rangle_A + |\psi(4\tau+2T_d)\rangle_B$, where

$$
\begin{aligned}
|\psi(4\tau+2T_d)\rangle_A &= \frac{-i}{2}\exp(-i\omega_{PA}(4\tau+2T_d))(-i\,|g,N'\rangle + |e,N'-1\rangle),\\
|\psi(4\tau+2T_d)\rangle_B &= \frac{-1}{2}\exp(-i\omega_{PA}(4\tau+2T_d))(|g,N'\rangle - i\,|e,N'-1\rangle).
\end{aligned}
\tag{1}
$$

The two arms, thus, yield identical proportions of $|g,N'\rangle$ and $|e,N'-1\rangle$. The probability of finding the atom in the ground state, which is the signal for the CRAI, is therefore, $S_{CRAI} = 1$. However, if the entire system is rotating at the rate Ω_G about an axis perpendicular to the area carved by the interferometer, a time delay, ΔT is introduced between the two paths. To consider its effect on the signal of the CRAI, we note that the state of the system at $t = 3\tau+2T_d$ is such that

$$
\begin{aligned}
|\psi(3\tau+2T_d)\rangle_A &= \frac{-i}{\sqrt{2}}\exp(-i\omega_{PA}(3\tau+2T_d))\exp(i(\omega_{C,g}+\omega_{C,e})\Delta T/4)\,|e,N'-1\rangle\,,\\
|\psi(3\tau+2T_d)\rangle_B &= \frac{-1}{\sqrt{2}}\exp(-i\omega_{PA}(3\tau+2T_d))\exp(-i(\omega_{C,e}+\omega_{C,g})\Delta T/4)\,|g,N'\rangle\,.
\end{aligned}
\tag{2}
$$

Finally, the state of the system due to rotation at the end of the $\pi/2$-dark-π-dark-$\pi/2$ sequence is such that

$$
\begin{aligned}
|\psi(4\tau+2T_d)\rangle_A &= \frac{-i}{2}\exp(-i\omega_{PA}(4\tau+2T_d))\exp(i\omega_{C,avg}\Delta T/2)(-i\,|g,N'\rangle + |e,N'-1\rangle),\\
|\psi(4\tau+2T_d)\rangle_B &= \frac{-1}{2}\exp(-i\omega_{PA}(4\tau+2T_d))\exp(-i\omega_{C,avg}\Delta T/2)(|g,N'\rangle - i\,|e,N'-1\rangle),
\end{aligned}
\tag{3}
$$

where $\omega_{C,avg} = (\omega_{C,g}+\omega_{C,e})/2$. The probability of finding the atom in the ground state, which is the signal for the CRAI, is therefore given by $S_{CRAI} = \cos^2(\Delta\phi/2)$, where $\Delta\phi = \omega_{C,avg}\Delta T$. From the special relativistic addition of velocities along the two trajectories, the time delay is found to be $\Delta T = 2\theta\Omega_G/c^2$, where θ is the area enclosed by the CRAI [3]. In a real experiment, one makes use of a laser, which is a coherent state, and not a Fock state.

However, when the mean photon number in the laser is very large, the excitation is akin to what we described here. In effect, the laser in this limit can be viewed effectively as a Fock state with a photon number equaling the mean photon number in the laser. This is the semiclassical approximation, where the quantum state of the field is assumed to remain unchanged (and thus factorized) independent of the state of the atom.

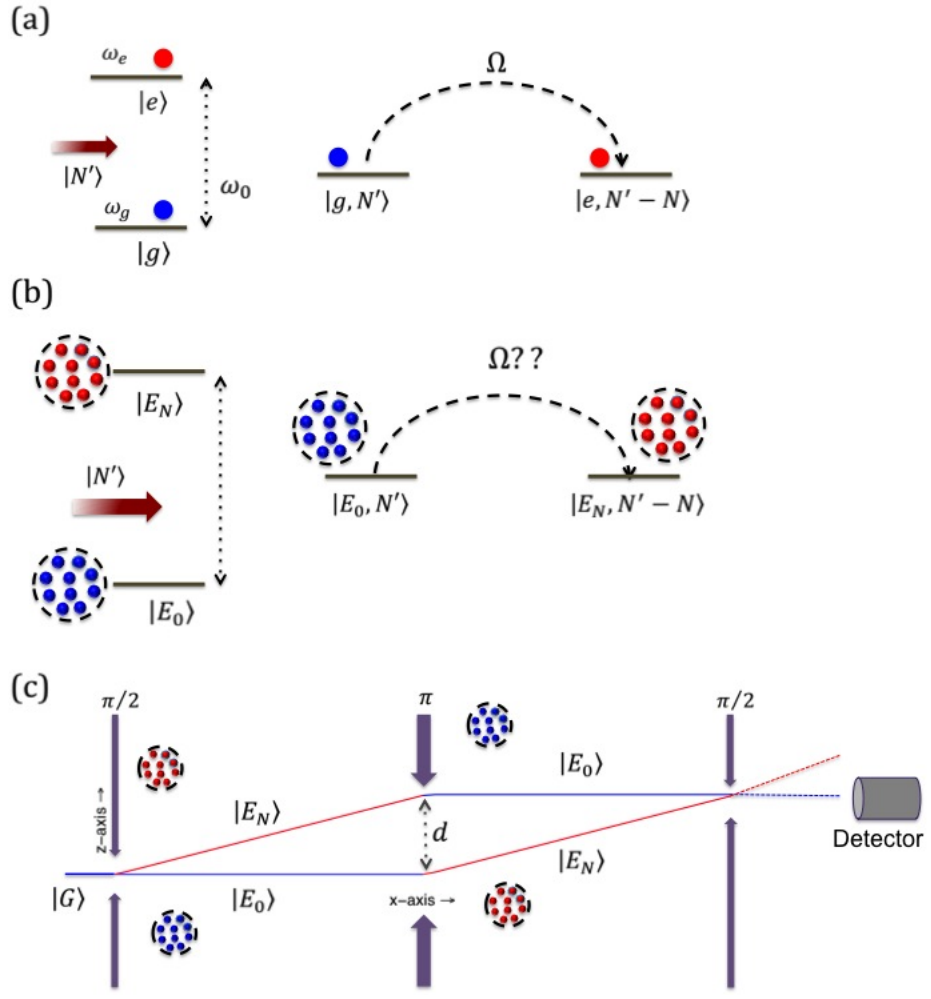

FIG. 1. (a) Single atom coupled to an N'-photon state, (b)N-atom ensemble coupled to an N'-photon state, (c) Ensemble interferometer formed by splitting and recombining of $|E_0\rangle$ and $|E_N\rangle$.

Next, we consider an ensemble of N such two level atoms that are independent and non-interacting. Furthermore, we consider the product state of this ensemble and a Fock state of N' photon as described above. Initially, all the atoms are in the state $|g\rangle$, so that the state of the ensemble-photon system is $|E_0\rangle\,|N'\rangle \equiv |E_0, N'\rangle$, where $|E_0\rangle = |g_1, g_2, \ldots, g_N\rangle$. Now, let us imagine a scenario (which is impossible in practice) that the state $|E_0, N'\rangle$ is

directly coupled to the state $|E_N, N'-N\rangle$ via the exchange of N photons between the states, where $|E_N\rangle = |e_1, e_2, \ldots, e_N\rangle$ as illustrated in 1(b). Such a process can be used to realize an atomic interferometer in a manner analogous to the CRAI, as illustrated in 1(c). The area enclosed in this case would be the same as that for a CRAI. However, the average Compton frequency will now be $N\omega_{C,avg}$ (and the de Broglie wavelength will be $\lambda_{dB,SingleAtom}/N$), so that the signal given by the population of state $|E_0\rangle$ measured at the end, will be $S_{ensemble} = \cos^2(N\Delta\phi/2)$, where $\Delta\phi$ is the phase shift experienced by a CRAI for the same amount of rotation.

However, since the electric dipole moment for a superposition of $|E_0\rangle$ and $|E_N\rangle$ vanishes, there is no way to realize the type of excitation envisioned above. Instead, when excited by a Fock state of $N'(> N)$ photons, this ensemble unfolds into a superposition of $(N+1)$ symmetric collective states given by $|E_n\rangle\,|N'-n\rangle$, where $|N'-n\rangle$ is a state of the field with $(N'-n)$ photons and $|E_n\rangle = J(N,n)^{-1/2}\sum_{k=1}^{J(N,n)} P_k\,|g^{\otimes(N-n)}e^{\otimes n}\rangle$, $J(N,n) = \binom{N}{n}$, P_k is the permutation operator, and $n = 0, 1, 2, \ldots, N$ [6]. The state $|E_n\rangle$ couples to its adjacent states via a single photon, and each laser interaction imparts it a momentum $n\hbar k$ in the direction of the beam. Some of these states and their relevant couplings are illustrated in Fig. 2. For example, state $|E_0, N'\rangle$ is coupled to the state $|E_1, N'-1\rangle$ at the rate of $\sqrt{N}\Omega_{N'}$, where $\Omega_{N'} = \sqrt{N'}\Omega_0$, with Ω_0 being the single-photon Rabi frequency (for exciting a single atom) and the $\sqrt{N}$ factor results from the collective enhancement of coupling. If the excitation is carried out by a laser field where the mean photon number is much larger than N, then we can make a semiclassical approximation that $\Omega_{N'} \cong \Omega_{N'-1} \cong \ldots \cong \Omega_{N'-N} \equiv \Omega$. Furthermore, the quantum state of the laser remains unchanged, (and thus factorized) independent of the state of the ensemble. The Compton frequency of the state $|E_n\rangle$ is given by $\omega_{C,En} = m_{En}c^2/\hbar$, where $m_{En} = m_{E0} + n\hbar\omega/c^2$ is the rest mass of the ensemble in state $|E_n\rangle$, and $m_{E0} = Nm$ is the rest mass of the ensemble in state $|E_0\rangle$. Thus, the dressed frequency of the ensemble-photon system ω_{PE}, which is a constant for all possible states of the system can be written as $\omega_{PE}(N, N') = m_{En}c^2/\hbar + (N'-n)\omega = m_{E0}c^2/\hbar + N'\omega$.

In the absence of an effective detuning, the CSAI is based on the coherent splitting and recombining of all of these symmetric collective states. To illustrate the mechanism behind the CSAI, we now consider the simplest ensemble: an assembly of two atoms of the kind described above and N' photons. At $t = 0$, the ensemble-photons system is assumed to be in the state $|E_0, N'\rangle$. The atom-field interaction couples it to the state $|E_1, N'-1\rangle$,

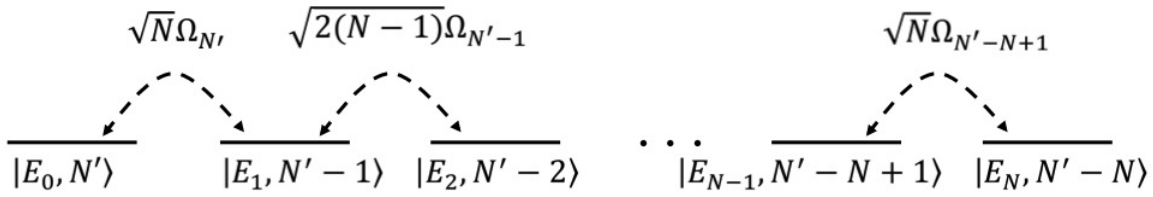

FIG. 2. Coupling between an N-atom ensemble symmetric collective states and N' photons.

which in turn is coupled to the state $|E_2, N'-2\rangle$. Following the notations of the $\pi/2$-dark-π-dark-$\pi/2$ sequence established for the CRAI, the state of the ensemble after the first $\pi/2$ pulse is $|\Psi(\tau)\rangle = \exp(-i\omega_{PE}\tau)(|E_0, N'\rangle_A - i\sqrt{2}\,|E_1, N'-1\rangle_B - |E_2, N'-2\rangle_C)/2$, where $\omega_{PE} \equiv \omega_{PE}(2, N')$ and the subscripts A, B, and C denote the lower, middle and upper trajectories of the interferometer, respectively, as shown in Fig. 3. This is followed by a dark zone of duration T_d, at the end of which the state of the ensemble is $|\Psi(\tau + T_d)\rangle = \exp(-i\omega_{PE}T_d)\,|\Psi(\tau)\rangle$. The component $|E_1, N'-1\rangle_B$ is displaced by $\hbar k T_d/2m$ along the $\mathbf{z}$-axis since it has absorbed the recoil from one photon ($\hbar k$), and it has a mass of $2(m_{C,g} + m_{C,e}) \approx 2m$. Similarly, $|E_2, N'-2\rangle$ is displaced by $\hbar k T_d/m$ along the $\mathbf{z}$-axis since it has absorbed recoils from two photons ($2\hbar k$), and it has a mass of $2m_{C,e} \approx 2m$. At $t = \tau + T_d$, the system interacts with the π-pulse (of duration 2τ) which causes the transition $|E_0, N'\rangle \leftrightarrow |E_2, N'-2\rangle$. The state $|E_1, N'-1\rangle$, however only picks up a phase due to the π interaction, and its trajectory remains unchanged. Explicitly, the state of the system at the end of the π-pulse is $|\Psi(3\tau + T_d)\rangle = |\Psi(3\tau + T_d)\rangle_A + |\Psi(3\tau + T_d)\rangle_B + |\Psi(3\tau + T_d)\rangle_C$, where

$$
\begin{aligned}
|\Psi(3\tau + T_d)\rangle_A &= -\exp(-i\omega_{PE}(3\tau + T_d))\,|E_2, N'-2\rangle\,/2, \\
|\Psi(3\tau + T_d)\rangle_B &= -\exp(-i\omega_{PE}(3\tau + T_d))\,|E_1, N'-1\rangle\,/\sqrt{2}, \\
|\Psi(3\tau + T_d)\rangle_C &= \exp(-i\omega_{PE}(3\tau + T_d))\,|E_0, N'\rangle\,/2.
\end{aligned} \tag{4}
$$

At the end of this pulse, the system passes through a second dark zone of duration T_d, which causes the state of the system to become $|\Psi(3\tau + 2T_d)\rangle = |\Psi(3\tau + 2T_d)\rangle_A + |\Psi(3\tau + 2T_d)\rangle_B + |\Psi(3\tau + 2T_d)\rangle_C$, where $|\Psi(3\tau + 2T_d)\rangle_A = \exp(-i\omega_{PE}T_d)\,|\Psi(3\tau + T_d)\rangle_A$, $|\Psi(3\tau + 2T_d)\rangle_B = \exp(-i\omega_{PE}T_d)\,|\Psi(3\tau + T_d)\rangle_B$, and $|\Psi(3\tau + 2T_d)\rangle_C = \exp(-i\omega_{PE}T_d)\,|\Psi(3\tau + T_d)\rangle_C$. By the end of this dark zone, the three trajectories converge and a last $\pi/2$-pulse is applied

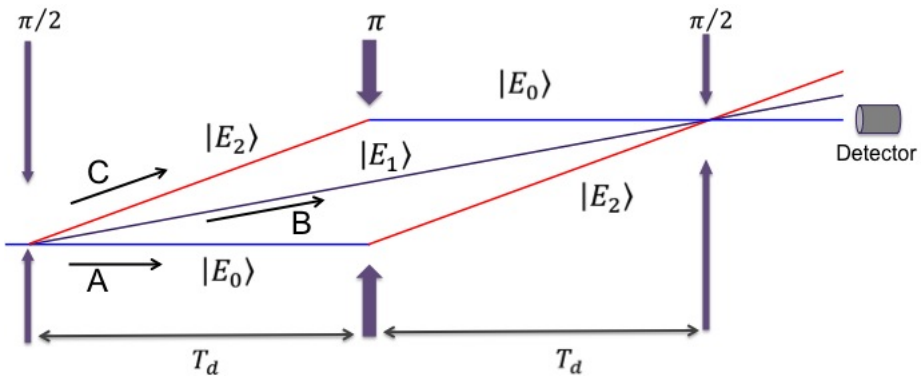

FIG. 3. Illustration of a two atom CSAI depicting the state trajectories.

which causes each of the trajectories to further split as follows:

$$
\begin{aligned}
|\Psi\rangle_A &= \frac{-1}{4}\exp(-i\omega_{PE}(4\tau+2T_d))(-|E_0,N'\rangle - i\sqrt{2}\,|E_1,N'-1\rangle + |E_2,N'-2\rangle),\\
|\Psi\rangle_B &= \frac{1}{2}\exp(-i\omega_{PE}(4\tau+2T_d))(|E_0,N'\rangle + |E_2,N'-2\rangle),\\
|\Psi\rangle_C &= \frac{1}{4}\exp(-i\omega_{PE}(4\tau+2T_d))(|E_0,N'\rangle - i\sqrt{2}\,|E_1,N'-1\rangle - |E_2,N'-2\rangle).
\end{aligned}
\tag{5}
$$

The signal of the CSAI is the probability of finding the ensemble in any of the collective states. We choose to measure the probability of $|E_0,N'\rangle$ for reasons discussed in the main body of the paper. The probability of finding the ensemble in state $|E_0,N'\rangle$, is therefore, $S_{CSAI}=1$. However, as explained above for the case of the CRAI, if the entire system is rotating at the rate Ω_G about an axis perpendicular to the area carved by the interferometer, a time delay is introduced between the paths. This time delay depends only on the area enclosed and the rate of rotation, as noted earlier. Let us assume that the delay between the paths C and A, which forms the $A-C$ loop, is ΔT. Therefore, the delay between paths B and A which form the $A-B$ loop, will be $\Delta T/2$. Similarly, the delay between paths C and B, which form the $B-C$ loop, will also be $\Delta T/2$. Since only the relative delay between two paths matter, we assume, for simplicity, that there is no delay on path B. Thus, just before the final $\pi/2$ pulse, we can write the quantum states of these paths under rotation as $|\Psi\rangle_{BR} = |\Psi(3\tau+2T_d)\rangle_B$, $|\Psi\rangle_{AR} = \exp(i(\omega_{C,E0}+\omega_{C,E2})\Delta T/4)\,|\Psi(3\tau+2T_d)\rangle_A$, and $|\Psi\rangle_{CR} = \exp(-i(\omega_{C,E2}+\omega_{C,E0})\Delta T/4)\,|\Psi(3\tau+2T_d)\rangle_C$. The last $\pi/2$-pulse causes each of these components to further split so that the state of the system at the end of the $\pi/2$-

dark-π-dark-$\pi/2$ sequence is

$$
\begin{aligned}
|\Psi\rangle_{AR} &= \frac{-1}{4}\exp(-i\omega_{PE}(4\tau+2T_d))\exp(i(\omega_{C,E0}+\omega_{C,E2})\Delta T/4) \\
&\quad\times(-|E_0,N'\rangle - i\sqrt{2}\,|E_1,N'-1\rangle + |E_2,N'-2\rangle), \\
|\Psi\rangle_{BR} &= \frac{1}{2}\exp(-i\omega_{PE}(4\tau+2T_d))(|E_0,N'\rangle + |E_2,N'-2\rangle), \\
|\Psi\rangle_{CR} &= \frac{1}{4}\exp(-i\omega_{PE}(4\tau+2T_d))\exp(-i(\omega_{C,E2}+\omega_{C,E0})\Delta T/4) \\
&\quad\times(|E_0,N'\rangle - i\sqrt{2}\,|E_1,N'-1\rangle - |E_2,N'-2\rangle).
\end{aligned}
\tag{6}
$$

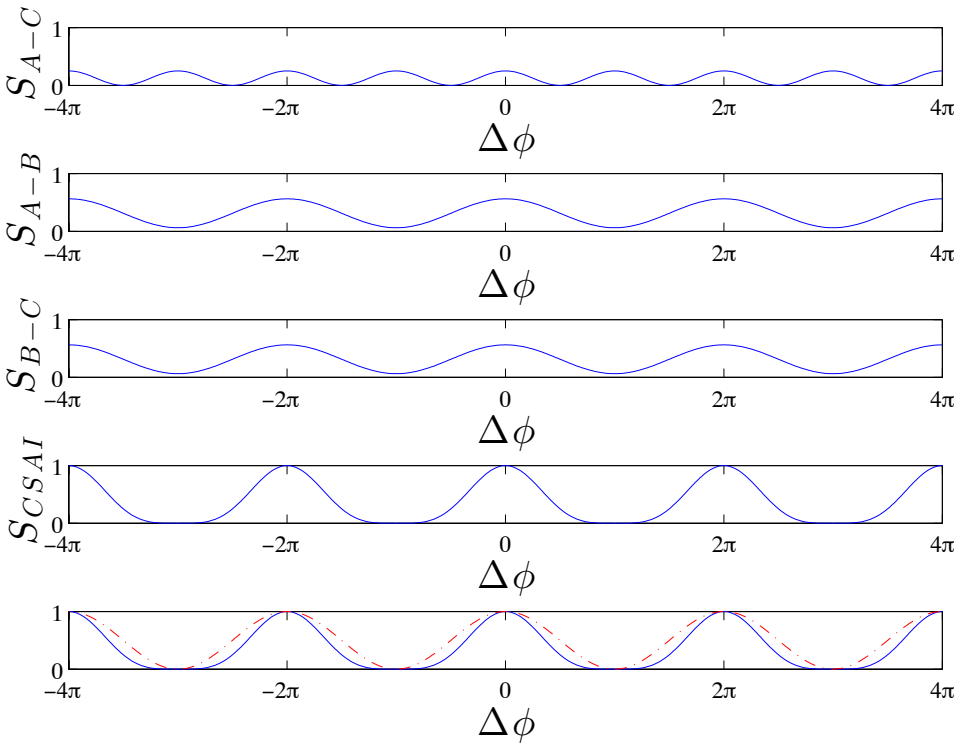

FIG. 4. Signals derieved from the interferometers formed by trajectories $A-C$, $A-B$, and $B-C$ and compared to the signal of the CSAI. The bottom panel shows the signal of CRAI in red compared to the signal of a 2-atom CSAI in blue.

The signal of the CSAI can, thus, be viewed as the aggregation of interference patterns due to three independent CRAI's working simultaneously., i.e. those formed by paths $A-B$, $B-C$ and $A-C$. To illustrate this, we denote the component of $|E_0,N'\rangle$ in paths A, B and C as χ_A, χ_B and χ_C, respectively. The interferometer formed by $A-B$ and $B-C$ are identical. The measurement of the amplitude of $|E_0,N'\rangle$ from each of these interferometers

is given by $S_{A-B} = S_{B-C} = |\chi_A + \chi_B|^2 = |\chi_B + \chi_C|^2 = 3/16 + \cos^2(\omega_{C,avg}\Delta T/2)/4$. This corresponds to a CRAI that is operating with an atom of average Compton frequency $\omega_{C,avg}$. The interferometer formed by $A - C$ yields the signal value $S_{A-C} = |\chi_A + \chi_C|^2 = \cos^2(\omega_{C,avg}\Delta T)/4$, behaving analogously to a CRAI formed by an atom of average Compton frequency $2\omega_{C,avg}$. The total CSAI signal arises due to the interference of the component of $|E_0, N'\rangle$ from the three paths, $S_{CSAI} = |\chi_A + \chi_B + \chi_C|^2 = \cos^4(\omega_{C,avg}\Delta T/2)$, as shown in Fig 4. This is reconciled by the fact that $|\chi_A + \chi_B + \chi_C|^2 = |\chi_A + \chi_B|^2 + |\chi_B + \chi_C|^2 + |\chi_A + \chi_C|^2 - (|\chi_A|^2 + |\chi_B|^2 + |\chi_C|^2)$.

II. PARAMETER INHOMOGENEITIES AFFECTING SIGNAL

In this section, we present a detailed description of the effect of inhomogeneity in Rabi frequency and Doppler shift on the signal of a CSAI. These inhomogeneities put significant constraints on the ensemble size, temperature of the trapped atoms, and the intensity profile and size of the laser beams. The manifestations of these effects can be analyzed by considering an ensemble of N identical non-interacting and independent atoms of the type described in Sec. I, as well as the main body of the paper. A laser beam propagating along the $\mathbf{z}$-axis will impart a momentum $\hbar k$ to an atom upon absorption of recoil from a single photon, driving it to a superposition of the states $|g_i, 0\rangle$ and $|e_i, \hbar k\rangle$, with the amplitude of each state depending on the intensity of the laser beam and the time of interaction. The field amplitude of the laser beams are assumed to be of Gaussian profile in $\mathbf{x}$ and $\mathbf{y}$ directions, and constant in the $\mathbf{z}$ direction. At $t = 0$, the position of the i-th atom is given by $\tilde{\mathbf{r}} = x_i\hat{\mathbf{x}} + y_i\hat{\mathbf{y}} + z_i\hat{\mathbf{z}}$. Due to the thermal motion of the atoms, each atom experiences a different Doppler shift and therefore, a different effective laser frequency, ω_{0i}. The net consequence of this is that the i-th atom picks up a detuning of $\delta_i = k\mathbf{v_{iz}}$, where $\mathbf{v_{iz}}$ denotes the atom's velocity in the $\mathbf{z}$-direction. Furthermore, each atom sees a different electric field, $\mathbf{E_i} = \hat{\mathbf{x}}E_0 \exp(-(x_i^2 + y_i^2)/2/\sigma_L^2)\cos(\omega_{0i}t - kz_i)$, due to the finite extent of the ensemble. Here σ_L represents the width of the laser beam in the transverse directions. Therefore, the Rabi frequency experienced by the i-th atom is given by $\Omega_i = \Omega_0 \exp[-(x^2+y^2)/2\sigma_L^2]$, where $\Omega_0 \equiv \langle g_i| (\mathbf{x} \cdot \rho_\mathbf{i}) |e_i\rangle E_0/\hbar = \langle e_i| (\mathbf{x} \cdot \rho_\mathbf{i}) |g_i\rangle E_0/\hbar$ and ρ_i is the position of the electron with respect to the nucleus.

In the electric dipole approximation, the Hamiltonian for the i-th atom can be written

as $H_i = |\mathbf{p}_i|^2/2m + H_{0i} + q\rho_\mathbf{i}.\mathbf{E_i}$, where H_{0i} is the internal energy of the atom, q is the electronic charge, m is the mass of the atom, and $\mathbf{p_i}$ is the momentum of the i-th atom. The COM motion kinetic energy term be expressed as $|\mathbf{p}_i|^2/2m = |\mathbf{p}_{iz}|^2/2m + |\mathbf{p}_{i\perp}|^2/2m$, where $\mathbf{p}_{iz}$ is the momentum in the $\mathbf{z}$ direction, and $\mathbf{p}_{i\perp}$ is the momentum in a direction perpendicular to $\mathbf{z}$. Consider first the effect of the second term: $|\mathbf{p}_{i\perp}|^2/2m$. In a typical experimental scenario, this accounts for the motion of the atom, typically at a large velocity, in the $\mathbf{x}$-direction (see Fig. 1 in the main body), acquired, for example by the initial push imparted to the trapped atoms before they enter the first interaction zone. Thus, any variation in this due to a velocity spread within the ensemble can be ignored, and this term can be treated as an overall constant energy which can be subtracted from the Hamiltonian. Consider next the first term: $|\mathbf{p}_{iz}|^2/2m$. This term shows that the state $|g, \mathbf{p_{iz}}\rangle$ coupled to $|e, \mathbf{p_{iz}} + \hbar k\rangle$ by the laser differ in energy by $(\hbar k v_{iz} + \hbar^2 k^2/2m)$, where the first term is the Doppler shift and the second term is the recoil energy which is a constant for all atoms, and can be subtracted from the Hamiltonian. Thus, after subtraction of constant terms, the net effect of the kinetic energy term is to account for the Doppler shift. Finally, as we have shown in detail in 7, a fully quantum mechanical description of the COM motion (e.g., by keeping track explicitly of the momentum of the atoms in the $|g\rangle$ and $|e\rangle$ states) is not essential in describing the collective states in the limit where the Rabi frequency of the i-th atom, Ω_i, is large compared to the Doppler shift due to the COM motion. This regime is valid for the CSAI, and, therefore, a semiclassical description of the COM motion of each atom suffices for the case at hand. Upon making the rotating-wave approximation, H_i can then be expressed in the bases of $|g_i\rangle$ and $|e_i\rangle$ as $H_i/\hbar = \omega_g |g_i\rangle \langle g_i| + \omega_e |e_i\rangle \langle e_i| + \Omega_i(\exp(i(\omega_{0i}t - kz_i)) |g_i\rangle \langle e_i| + h.c.)/2$, where ω_e includes the Doppler shift. Performing the rotating-wave transformation and removing any phase factors causes the transformation $H_i \rightarrow H_i'$, such that $H_i'/\hbar = -\delta_i |e_i'\rangle \langle e_i'| + \Omega_i(|g_i'\rangle \langle e_i'| + h.c.)/2$. The new basis vectors, $|g_i'\rangle$ and $|e_i'\rangle$, are related to the original basis vectors as $\exp(-i\omega_g t) |g_i\rangle$ and $\exp(-i((\omega_e + \delta_i)t - kz_i)) |e_i\rangle$, respectively. Assuming that the i-th atom is initially in the state $c_{gi}(0) |g_i'\rangle + c_{ei}(0) |e_i'\rangle$, its quantum state can be written as

$$
\begin{aligned}
|\psi_i'\rangle =& e^{i\delta_i t/2}((c_{gi}(0)\cos\left(\frac{\Omega_i' t}{2}\right) - i\frac{c_{gi}(0)\delta_i + c_{ei}(0)\Omega_i}{\Omega_i'}\sin\left(\frac{\Omega_i' t}{2}\right))|g_i'\rangle \\
&+ (-i\frac{c_{gi}(0)\Omega_i - c_{ei}(0)\delta_i}{\Omega_i'}\sin\left(\frac{\Omega_i' t}{2}\right) + c_{ei}(0)\cos\left(\frac{\Omega_i' t}{2}\right))|e_i'\rangle), \qquad (7)
\end{aligned}
$$

where $\Omega_i' = \sqrt{\Omega_i^2 + \delta_i^2}$ is the effective coupling frequency of this atom. The relative separation of the atoms along the direction of propagation of the laser beam has no effect on the fidelity of the collective states that can be attained by the ensemble [7]. For the purpose of the present discussion, we stay in the bases of $|g_i'\rangle$ and $|e_i'\rangle$.

At $t = 0$, the first pulse of duration τ is applied to the atoms so that $\Omega_0\tau = \pi/2$. The state of the i-th atom following this interaction can be written as $|\psi_i'(\tau)\rangle = c_{gi}(\tau)\,|g_i'\rangle_A + c_{ei}(\tau)\,|e_i'\rangle_B$, where $c_{gi}(\tau) = \exp(i\delta_i\tau/2)((\cos(\Omega_i'\tau/2) - i\delta_i\sin(\Omega_i'\tau/2)/\Omega_i')$ and $c_{ei}(\tau) = \exp(i\delta_i\tau/2)(-i\Omega_i\sin(\Omega_i'\tau/2)/\Omega_i')$. The subscripts A and B denote the lower and upper arm of the interferometer trajectory. The ensuing dark zone lasts for a duration T_d wherein the atoms are left to drift freely so that at $t = \tau + T_d$, the COM of state $|e_i'\rangle$ is separated from that of state $|g_i\rangle$ by $d = \hbar k T_d/m$. During this dark zone where no atom-light interaction is taking place, the portion of the atom in state $|e_i'\rangle$ picks up a phase due to detuning, making the state of the atom at the end of this pulse $|\psi_i'(\tau + T_d)\rangle = c_{gi}(\tau + T_d)\,|g_i'\rangle_A + c_{ei}(\tau + T_d)\,|e_i'\rangle_B$, where $c_{gi}(\tau + T_d) = c_{gi}(\tau)$ and $c_{ei}(\tau + T_d) = \exp(i\delta_i T_d)c_{ei}(\tau)$. At this point a second pulse of duration 2τ (π-pulse) is applied to atoms, and each trajectory undergoes further splitting, as shown in Fig.1 in the main body of this paper. The π-pulse can, in principle, be perfect only for one group of atoms, such as those with $\delta = 0$. For all other atoms, the pulse duration will differ slightly from π. As a result, for example, the $|e_i'\rangle$ state will not fully evolve into the $|g_i'\rangle$ state, and a residual amount will stay in the $|e_i'\rangle$ state. In the regime where $\Omega_i \gg \delta_i$ for all i, the effect of these residual components can be safely ignored. Under this approximation, the state of the atom is given by $|\psi_i'(3\tau + T_d)\rangle = c_{ei}(3\tau + T_d)\,|e_i'\rangle_A + c_{gi}(3\tau + T_d)\,|g_i'\rangle_B$, where $c_{ei}(3\tau + T_d) = \exp(i\delta_i\tau)c_{gi}(\tau + T_d)(-i\Omega_i\sin(\Omega_i'\tau)/\Omega_i')$ and $c_{gi}(3\tau + T_d) = \exp(i\delta_i\tau)c_{ei}(\tau + T_d)(-i\Omega_i\sin(\Omega_i'\tau)/\Omega_i')$. Following the π-pulse, the atoms are further set adrift in another dark zone of duration T_d, where the component of the atom following trajectory A picks up a phase due to detuning. The net effect of this is that $|\psi_i'(3\tau + 2T_d)\rangle = c_{ei}(3\tau + 2T_d)\,|e_i'\rangle_A + c_{gi}(3\tau + 2T_d)\,|g_i'\rangle_B$, where $c_{ei}(3\tau + 2T_d) = \exp(i\delta_i T_d)c_{ei}(3\tau + T_d)$ and $c_{gi}(3\tau + 2T_d) = c_{ei}(3\tau + T_d)$. By the end of this dark zone, the two trajectories converge and a third pulse of duration τ is applied to the atoms. Therefore, the state of the atom at $t = 4\tau + 2T_d$ is $|\psi_i'(4\tau + 2T_d)\rangle = (c_{gi}(4\tau + 2T_d)_A\,|g_i'\rangle + c_{ei}(4\tau + 2T_d)_A\,|e_i'\rangle) + (c_{gi}(4\tau + 2T_d)_B\,|g_i'\rangle + c_{ei}(4\tau + 2T_d)_B\,|e_i'\rangle)$, where $c_{gi}(4\tau + 2T_d)_A = \exp(i\delta_i\tau/2)c_{ei}(3\tau + 2T_d)(-i\Omega_i\sin(\Omega_i'\tau/2)/\Omega_i')$, $c_{ei}(4\tau + 2T_d)_A = \exp(i\delta_i\tau/2)c_{ei}(3\tau + 2T_d)(\cos(\Omega_i'\tau/2) + i\delta_i\sin(\Omega_i'\tau/2)/\Omega_i')$, $c_{gi}(4\tau + 2T_d)_B = \exp(i\delta_i\tau/2)c_{gi}(3\tau + 2T_d)(\cos(\Omega_i'\tau/2) -$

$i\delta_i \sin(\Omega_i'\tau/2)/\Omega_i')$, and $c_{ei}(4\tau + 2T_d)_B = \exp(i\delta_i\tau/2)c_{gi}(3\tau + 2T_d)(-i\Omega_i \sin(\Omega_i'\tau/2)/\Omega_i')$.

The signal of the CRAI formed by the i-th atom is the measurement of the amplitude of state $|g_i'\rangle$ at the end of the $\pi/2$-dark-π-dark-$\pi/2$ sequence due to the interference of the components from the two paths. Since the two arms yield identical proportions of both $|g_i'\rangle$ and $|e_i'\rangle$, i.e. $c_{gi}(4\tau + 2T_d)_A = c_{gi}(4\tau + 2T_d)_B$ and $c_{ei}(4\tau + 2T_d)_A = -c_{ei}(4\tau + 2T_d)_B$, the signal of the CRAI formed is $S_{CRAI,i} = \alpha_i$, where $\alpha_i = |2c_{gi}(4\tau + 2T_d)_A|^2 \leq 1$. Since the signal of a CSAI is the product of the signals of the individual CRAI's formed by the constituent atoms in the ensemble [7], the signal of the resulting CSAI is, consequently, $S_{CSAI} = \prod_i^N S_{CRAI,i} = \prod_i^N \alpha_i$. However, if a phase difference is introduced between the two paths, the signal of the CRAI's and thus, the CSAI will depend on it additionally. Assuming that an external phase, $\Delta\phi$ is introduced to the path A of the interferometer, the quantum state of the atom at $t = 4\tau + 2T_d$ is given by $|\psi_i'(4\tau + 2T_d)\rangle = \exp(i\Delta\phi)(c_{gi}(4\tau + 2T_d)_A |g_i'\rangle + c_{ei}(4\tau + 2T_d)_A |e_i'\rangle) + (c_{gi}(4\tau + 2T_d)_B |g_i'\rangle + c_{ei}(4\tau + 2T_d)_B |e_i'\rangle)$. The amplitude of $|g_i'\rangle$ will, thus, be $S_{CRAI,i} = |1 + \exp(-i\Delta\phi)|^2\alpha_i = 4\alpha_i \cos^2(\Delta\phi/2)$. In the case where $\Omega_i \gg \delta_i$, $\alpha_i = 1/4$ and the signal shows the well known $\cos^2(\Delta\phi/2)$ dependence. The resulting CSAI signal is, therefore, $S_{CSAI} = \prod_i^N 4\alpha_i \cos^2(\Delta\phi/2)$. In the ideal situation where each atom sees the same Rabi frequency due to a uniform beam profile and there is no effective detuning experienced by the atoms, $\alpha_i = 1/4$ and the signal at the end of the interferometer sequence is given by $S_{CSAI} = \cos^{2N}(\Delta\phi/2)$. This corresponds to the narrowing of the signal fringe by a factor proportional to $\sqrt{N}$ as compared to the signal in a CRAI.

In the more practical situation relevant for experimental conditions, Ω_i and δ_i for each atom are determined by the laser beam intensity profile, and atom trap size and temperature, as described above. To illustrate the effect of these parameters, we assume that the atoms are first cooled down using a magneto-optic trap arrangement. The trapped atoms are then held in a dipole trap to further cool them down via evaporative cooling. We assume that the density of atoms in the trap follows a Gaussian spatial distribution with a full width of ξ. The Maxwell-Boltzmann velocity distribution of the ensemble is $f_{MB}(v, T_{MB}) = \sqrt{m/2\pi k_B T_{MB}} \exp(-mv^2/2\pi k_B T_{MB})$, where T_{MB} is the temperature of the trap and k_B is the Boltzmann constant. The plot of S_{CRAI} for various values of N at $T_{MB} = 2\mu K$ average temperature of the trap is shown in Fig. 5(a). The signal peak value falls sharply with increasing N as illustrated in Fig 5(b). It is also evident from Fig. 5(c) that the signal of a CSAI varies significantly as a function of the temperature.

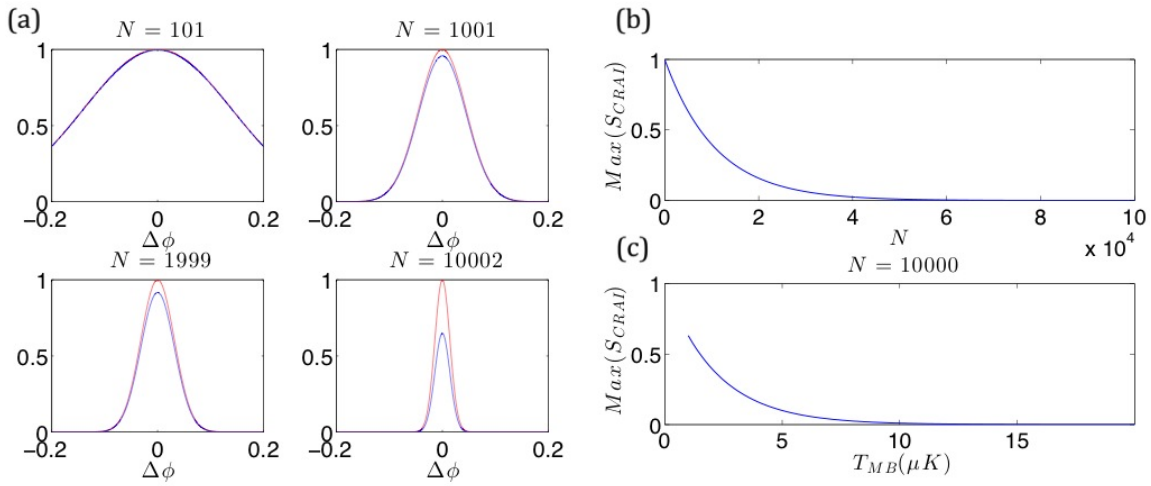

FIG. 5. (a) The signal at an average temperature of $2\mu K$ and rectangular intensity profile beams at $\Omega = 3.4 \times 10^7 \mathrm{s}^{-1}$ is shown in blue. The ideal signal with no Doppler shift induced detuning is shown in red. (b) Variation of signal peak value with N at 2μK average temperature. (c) Variation of signal peak value with trap temperature for $N \simeq 10^4$.

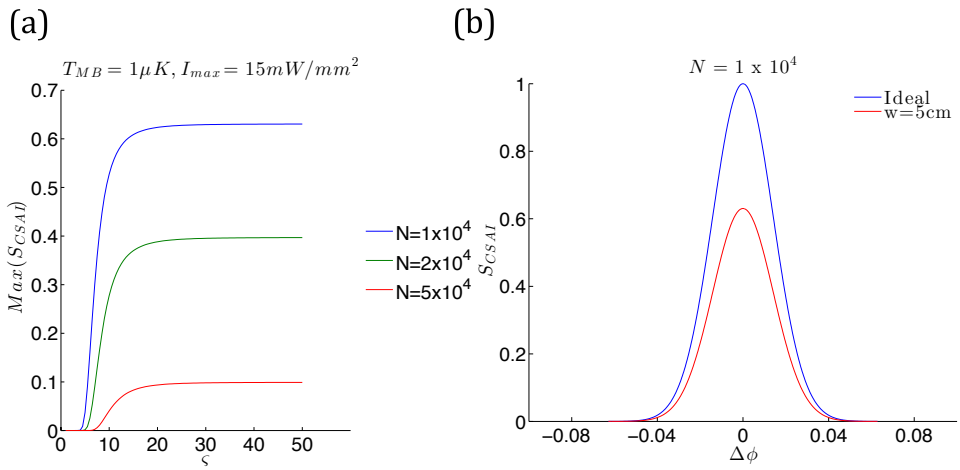

FIG. 6. (left) Variation of the peak value of the S_{CSAI} with increasing MOT size to beam waist ratio at $T_{MB} = 1\mu$K for different values of N. (right) The signal assuming $5cm$ beam waist size for $N = 1 \times 10^4$ is in red. The ideal signal assuming rectangular beam profile and no Doppler shift is shown in blue.

Next, we consider the effect of the Gaussian spatial distribution of the Raman beams on the CSAI. Assuming that the beam waist size is w, the Raman Rabi frequency experienced by the i-th atom of the ensemble is $\Omega_i = \Omega_0 \exp(-2r^2/w^2)$. Here Ω_0 is the peak value of the

Raman Rabi frequency and r is the radial distance of the i-th atom from the center of the beam. We consider that the average temperature of the trapped atoms is $T_{MB} = 1\mu$K and the peak value of the beam intensity is 5 mW/mm^2 so that $\Omega_0 = 1.14 \times 10^7$ rads^{-1}. Figure 6 shows the variation of the peak value of the S_{CSAI} with increasing value of $\varsigma = \xi/w$.

III. EFFECT OF SPONTANEOUS EMISSION

In our analysis of the CSAI, we have employed a model of a three-level atom where the intermediate state ($|a, \hbar k_1\rangle$) is adiabtically eliminated to reduce the system to an equivalent two-level model. However, the actual population of this state is non-zero. Consequently, the signal for both the CRAI and the CSAI would deviate from the ideal one. The effect of spontaneous emission on the CRAI can be taken into account by using the density matrix equation for a three level system. However, in this case, it is not possible to ascribe a well defined quantum state for each atom. This, in turn, makes it difficult to figure out the response of the CSAI, since our analysis for the CSAI is based on using the direct product of the quantum state of each atom. For a large value of N, it is virtually impossible to develop a manageable density matrix description of the system directly in terms of the collective states. However, it should be possible to evaluate the results of such a density matrix based model for a small value of N (< 10, for example). In the near future, we will carry out such a calculation and report the findings.

For the general case of large N, one must rely on an experiment (which, in this context, can be viewed as an analog computer for simulating this problem) to determine the degree of degradation expected from residual spontaneous emission. It should be noted that the deleterious effect of spontaneous emission, for both the CRAI and the CSAI, can be suppressed to a large degree by simply increasing the optical detuning while also increasing the laser power. This is the approach used, for example, in reducing the effect of radiation loss of atoms in a far off resonant trap (FORT).

IV. EFFECT OF QUANTUM AND CLASSICAL NOISE

For the CSAI to be a useful device for practical metrology, it must outperform the CRAI. To explore this, we compare their stability in the short term and the long term regimes. The

stability of an interferometer is determined by the fluctuations in $\Delta\phi$ that has both quantum mechanical and classical components. The phase difference, $\Delta\phi$ (expressed in radians) is proportional to the rate of rotation of the gyroscope, Ω_G (see Sec. I). Thus, $\Delta\phi = \mu\Omega_G$, where μ depends on the area of the interferometer and mass of the single atom.

In the CRAI described above, the signal is a measure of the probability of finding the atom in state $|g\rangle$, $P_g = \cos^2(\mu\Omega_G/2)$. The signal is detected by probing the desired state for a duration of time. If $\tilde{N}$ is the number of atoms per unit time and T is the interrogation period, then the net signal is $S_{CRAI} = \tilde{N}TP_g$. For comparison, we set the number of atoms per trial in the CSAI, N, multiplied by the number of trials, M, to equal $\tilde{N}T$. Therefore, $S_{CRAI} = MN\cos^2(\mu\Omega_G/2)$. Since the fluctuation in MN is $\sqrt{MN}$, the quantum mechanical variance of the signal is $\Delta(S_{CRAI,QM}) = \sqrt{MN}\sin(\mu\Omega_G)/2$, since the projection noise in a single two level atomic system is $\Delta S_{CRAI} = \sqrt{P_g(1-P_g)}$ [9]. In the case where the probability of finding the atom in $|g\rangle$ is 0 or 1, the projection noise vanishes. On the other hand, the projection noise is at its peak value when $P_g = 1/2$. The slope of the signal is, therefore, $\partial S_{CRAI}/\partial\Omega_G = -MN\sin(\mu\Omega_G)/(2\gamma_{sa})$, where $\gamma_{sa} = 1/2\mu$ is the linewidth. Assuming ideal quantum efficiency of the detection process, the fluctuation in the rate of rotation can be written as $\delta\Omega_G|_{total} = |(\Delta S_{QM} + \Delta S_{classical})/(\partial S_{CRAI}/\partial\Omega_G)|$, which maybe be considered as noise (ΔS), over the Rotational Variation of Signal (RVS) which is $(\partial S_{CRAI}/\partial\Omega_G)$. In the following text, we consider first the effect of quantum noise. The quantum rotation-rate fluctuation (QRF) for a CRAI maybe written as

$$\delta\Omega_G|_{QM,CRAI} = \left|\frac{\Delta S_{QM}}{(\partial S_{CRAI}/\partial\Omega_G)}\right| = \frac{\gamma_{sa}}{\sqrt{MN}}. \tag{8}$$

It is, thus, merely a coincidence that the QRF turns out to be constant in a CRAI. Contrary to popular perception, the QRF of an interferometer is, therefore, not fundamentally the linewidth divided by the signal-to-noise ratio (SNR). It should be evident from the above discussion that the signal is not given by MN, and the noise is not given by $\sqrt{MN}$. Instead, they both depend on Ω_G.

In devices where the QRF is not a constant, as we will show for a CSAI, it is thus, imperative that we carry out an analysis of the QRF in a manner analogous to the analysis for the CRAI shown above. Thus, we will adopt the approach that the net rotation-rate fluctuation, $\delta\Omega_G$ should be thought of as the ratio of the noise to the RVS. This approach should be adopted universally for all metrological devices. Of course, for devices where

the relevant quantity is not the rotation rate, the definition should be adapted accordingly. For example, in a clock that measures frequency, the relevant quantity can be expressed as follows: net frequency fluctuation is the ratio of the noise to the Spectral Variation of Signal (SVS).

Following this approach, we calculate the net rotation-rate fluctuation of the CSAI and compare it to that of the CRAI. We will first calculate the quantum fluctuation which is relevant in the short term regime, and then the classical fluctuation, which dominates in the long term regime. The signal of a CSAI for M trials is $S_{CSAI} = MP_{E0} = M\cos^{2N}(\mu\Omega_G/2)$, and the projection noise is $\Delta P_{E0} = \sqrt{P_{E0}(1-P_{E0})}$ for a single trial, so that $\Delta P_{E0} = \sqrt{M}\sqrt{P_{E0}(1-P_{E0})}$ for M trials. Thus, the total quantum mechanical noise in the signal is

$$\Delta P_{E0} = \sqrt{M}\cos^{N}(\mu\Omega_G/2)\sqrt{1-\cos^{2N}(\mu\Omega_G/2)}, \tag{9}$$

and the RVS is

$$\partial S_{CSAI}/\partial\Omega_G = -MN\cos^{2N-1}(\mu\Omega_G/2)\sin(\mu\Omega_G/2)/\gamma_{sa}. \tag{10}$$

Therefore, the QRF in the CSAI is given by

$$\delta\Omega_{G(QM,CSAI)} = \frac{\gamma_{sa}}{N\sqrt{M}}\frac{\sqrt{1-\cos^{2N}(\mu\Omega_G/2)}}{\cos^{N-1}(\mu\Omega_G/2)\sin(\mu\Omega_G/2)}. \tag{11}$$

Thus, unlike the CRAI, the phase fluctuation in a CSAI is not constant and depends on Ω_G and thus, on $\Delta\phi$. We consider first, the limiting case of $\Omega_G \to 0$. Using Taylor expansion, it is evident that $\delta\Omega_{G(QM,CSAI)} = \gamma_{sa}/\sqrt{MN}$, which is the same as that of a CRAI. This can be understood physically by noting that while the fringe width becomes much narrower for the CSAI, the SNR also decreases due to the fact that a single observation is made for all N atoms in a given trial. The QRF for the CSAI, given in Eq. 11, is smallest as $\Omega_G \to 0$ and increases as Ω_G moves away from zero. The ratio of the QRF for the CRAI to that of the CSAI is plotted as a function of Ω_G in the left side of Fig. 7 for $M = 1000$ and $N = 10^4$. Here, the vertical bars indicate the FWHM of the CSAI signal. It is clear from this plot that the QRF for the CSAI increases significantly as we move away from resonance. However, since a servo will keep the value of Ω_G confined to be close to zero, the phase stability of the CSAI, under quantum noise limited operation, should be very close to that of the CRAI, assuming that all the other factors remain the same.

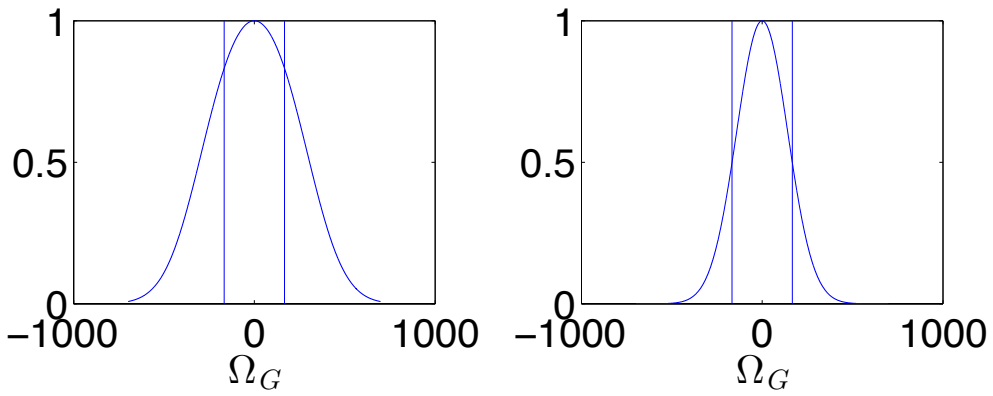

FIG. 7. (left) Ratio of the QRF in the CRAI to the QRF in the CSAI, for $M = 1000$ and $N = 10^4$. It should be noted that the fluctuation in the CRAI is independent of Ω_G while that of the CSAI varies significantly with it. (right) Ratio of the RVS of the CSAI to the RVS of the CRAI for $M = 1000$ and $N = 10^4$. The vertical lines in the plots show where the FWHM of S_{CRAI} are.

The classical rotation-rate fluctuation (CRF), $\delta\Omega_G|_{classical} = \Delta S_{classical}/(\partial S/\partial\Omega_G)$, is the limiting factor in the long term stability. While the quantum fluctuation is dominated by quantum projection noise, the classical noise is dominated by noise in the electronic and the mechanical components employed to generate the interferometer signal. Since the pieces of equipment used in the development of both the CSAI and CRAI suffer from similar noise issues, the variance ΔS is expected to be of the same order of magnitude for both interferometers. On the other hand, the RVS, $(\partial S/\partial\Omega_G)$, is not the same, as was shown previously. The ratio of the RVS of the CSAI to the RVS of the CRAI is

$$\frac{\partial S_{CSAI}/\partial\Omega_G}{\partial S_{CRAI}/\partial\Omega_G} = \frac{cos^{2N}(\mu\Omega_G/2)}{cos^2(\mu\Omega_G/2)} = \frac{P_{E0}}{P_g}, \tag{12}$$

and is plotted in Fig. 7(right). With $\Delta S_{classical,CSAI} \sim \Delta S_{classical,CRAI}$, the ratio of the CRF of the CSAI to that of the CRAI can be written as

$$\frac{\delta\Omega_{G(classical,CSAI)}}{\delta\Omega_{G(classical,CRAI)}} \simeq \frac{\cos^2(\mu\Omega_G/2)}{\cos^{2N}(\mu\Omega_G/2)}. \tag{13}$$

Similar to the ratio of the two interferometers in QRF, Eq. 13 is smallest as $\Delta\phi \to 0$ and increases as $\Delta\phi$ moves away from resonance. Thus, with respect to both quantum and classical sources of noise, the CSAI must be operated near $\Delta\phi \simeq 0$ for optimal performance.

V. EFFECT OF DETECTOR EFFICIENCY

The key aspect of the CSAI is the measurement of the amplitude of $|E_0\rangle$, which indicates that each of the atoms in the ensemble is individually in $|g\rangle$. At the end of the $\pi/2$-dark-π-dark-$\pi/2$ sequence, a fourth probe beam is applied to the ensemble to measure the amplitude of one of the resulting collective states, via the method of zero photon detection, as explained in the main body of the paper. The probe beam is applied to the ensemble, which is in the quantum state $|\Psi\rangle = c_0 |E_0\rangle + \sum_{n=1}^{N} |E_n\rangle$. Interaction between the probe beam, the ensemble, and the free space vacuum modes on the other leg would lead to production of photons unless $c_0 = 1$, and $c_n = 0$ for all n. These photons are detected using a heterodyning technique, as described in the main body of the paper. The voltage output of the heterodyning system is proportional to the amplitude of the electric field corresponding to the photons.

In general, one or more photons are produced as $|E_n\rangle$ decays to $|E_{n-1}\rangle$ and subsequent states. The time needed for these photons to be produced depends in the vacuum and probe field induced Raman transition rates between $|E_n\rangle$ and $|E_{n-1}\rangle$. If we assume perfect efficiency for detecting each of these photons, and wait for a time long compared to the inverse of the weakest of these transition rates, then the detection of no photons implies that the system is in state $|E_0\rangle$. In practical experimental conditions, we can choose a small threshold voltage at the output of the heterodyning system as an indicator of null detection. Thus, any signal below this threshold would be viewed as detection of the quantum system in the $|E_0\rangle$ state, and all signals above this threshold would be discarded. The number of events below this threshold for $\mathscr{M}$ trials carried out with all the parameters of the experiment unchanged, is the derived signal for the CSAI. After collecting data for all the values of $\Delta\phi$ that is of interest, the result would ideally yield the plot of the CSAI signal $S_{CSAI} = |c_0|^2$, averaged over $\mathscr{M}$ trials. However, with a fractional detector efficiency and finite detection period, the signal would deviate from the ideal result.

Consider first the effect of the detection period. Given the decay rate of the off-resonant Raman process, $\gamma_n = n(N + 1 - n)\gamma_{sa}$ as described in the main body, the probability that $|E_n\rangle$ will produce zero photons during the measurement period T is $P_{0,n} = e^{-\gamma_n T}$. Thus, the total probability of zero photon emission (which should vanish ideally for any $c_n \neq 0$) is given by $P_0 = \sum_{n=1}^{N} |c_n|^2 e^{-\gamma_n T}$. The CSAI signal, S_{CSAI}, is the total probability of finding zero photons during T, and can be expressed as $S_{CSAI} = |c_0|^2 + \sum_{n=1}^{N} |c_n|^2 e^{-\gamma_n T}$. Noting

that $\gamma_0 = 0$, we can rewrite this as $S_{CSAI} = \sum_{n=0}^{N} |c_n|^2 e^{-\gamma_n T}$. The lower and upper bounds of S_{CSAI} can be established by considering the strongest and the weakest effective decay rates. The strongest decay rate occurs for the middle state, $\gamma_{N/2} = (N/2)(N/2+1)\gamma_{sa} \approx (N^2/4)\gamma_{sa}$, where $N \gg 1$ approximation has been made. With the substitution of the largest decay rate for each $|E_n\rangle$ into the equation for S_{CSAI}, the lower bound is set by

$$P_L = |c_0|^2 + (1 - |c_0|^2) \exp(-N^2 \gamma_{sa} T/4). \tag{14}$$

On the other hand, the weakest decay rate is exhibited when $n = N$, making the upper bound on the signal,

$$P_U = |c_0|^2 + (1 - |c_0|^2) \exp(-N \gamma_{sa} T). \tag{15}$$

The signal of the CSAI, S_{CSAI} produced in time T will lie somewhere between P_L and P_U.

Consider next the effect of the non-ideal detection efficiency of the heterodyning scheme. For concreteness, we define η as the efficiency of detecting a single photon. In practice, this parameter will depend on a combination of factors, including the quantum efficiency of the high-speed photon detector and the overlap between the probe laser mode and the mode of the emitted photon. For the present experiment, we are only interested in knowing whether at least one photon is detected, and not in the actual number of photons. When more photons are emitted, the detector will have a better chance of observing a non-zero signal, and hence distinguish dark counts from the rest with more certainty. For example, if three photons are emitted in time T, then four different outcomes are possible:

- All three photons are detected, with probability η^3;
- Two of the photons are detected with probability $\eta^2(1-\eta)$; this can occur for any two of the photons, so the multiplicity is 3;
- One photon is detected, with probability $\eta(1-\eta)^2$ and multiplicity of 3;
- No photons are detected, with probability $\epsilon^3 \equiv (1-\eta)^3$.

The sum of these probabilities is 1. The probability that at least 1 photon is detected is thus $(1 - \epsilon^3)$. For any state $n \neq 0$, the probability of detecting at least 1 photon is, therefore, $(1 - \epsilon^n)$.

Moreover, we must also consider how the effective detection efficiency is influenced by the fact that the collective states decay at different rates. Specifically, the n level for $n > 0$

might produce $N-n$ photons, $N-n-1$ photons, down to zero photons, depending on the length of the measurement time and the effective decay rate. If the system is in $|E_3\rangle$, for example, it can produce up to 3 photons but with probabilities that change over T. For a given time T, $|E_3\rangle$ evolves into a sum of the states $|E_3\rangle \rightarrow \sum_{k=0}^{3} a_{n,k}(T)\,|E_k\rangle$, where the coefficient $a_{n,k}(T)$ depends on the effective decay rate that is specific to each state, and changes as the states evolve in time. Thus the probability of detecting at least one photon is

$$P = \sum_{n=1}^{N-1} |c_n|^2 \sum_{k=n}^{N} (1-\epsilon^{k-n}) |a_{n,k}(T)|^2. \tag{16}$$

Therefore, the probability of detecting no photon is

$$S_{CSAI} = 1 - P = 1 - \sum_{n=1}^{N-1} |c_n|^2 \sum_{k=n}^{N} (1-\epsilon^{k-n}) |a_{n,k}(T)|^2. \tag{17}$$

The numerical analysis for a large number of atoms is tedious and scales as at least $(N-1)!$ for the CSAI. However, we can take the worst case scenario to serve as the upper bound for the signal. The worst case occurs when only a single photon is produced as a result of $|E_n\rangle$ decaying to only the $|E_{n-1}\rangle$ state, so that the index of the second summation stops at $k = n-1$. In this case, we can write $|a_{n,n-1}(T)| = (1-e^{-\gamma_n T})$ and the signal becomes

$$S_{CSAI} = |c_0|^2 + \epsilon(1-|c_0|^2) + \eta \sum_{n=1}^{N} |c_n|^2 e^{-\gamma_n T}. \tag{18}$$

Using the approach we employed in arriving at Eq. 14 and Eq. 15, we now consider the strongest and the weakest decay rates for single photon production to arrive at the lower and upper bounds of the zero photon count signal:

$$P_L = 1 - \eta(1-|c_0|^2)(1-e^{-N^2\gamma_{sa}T/4}), \tag{19}$$

$$P_U = 1 - \eta(1-|c_0|^2)(1-e^{-N\gamma_{sa}T}). \tag{20}$$

Figure 8 shows the plot of the ideal S_{CSAI}, P_L and P_U over a variation in $\Delta\phi$ for different values of detector efficiencies and detection times for $N = 100$ and $N = 10,000$. It can be seen from the plots that the upper and lower bounds on the signal coincide with the ideal signal in the vicinity of $\Delta\phi \rightarrow 0$. For a larger size of the ensemble, a longer detection time ensures that the gap between the bounds decreases and that they are closer to the ideal signal.

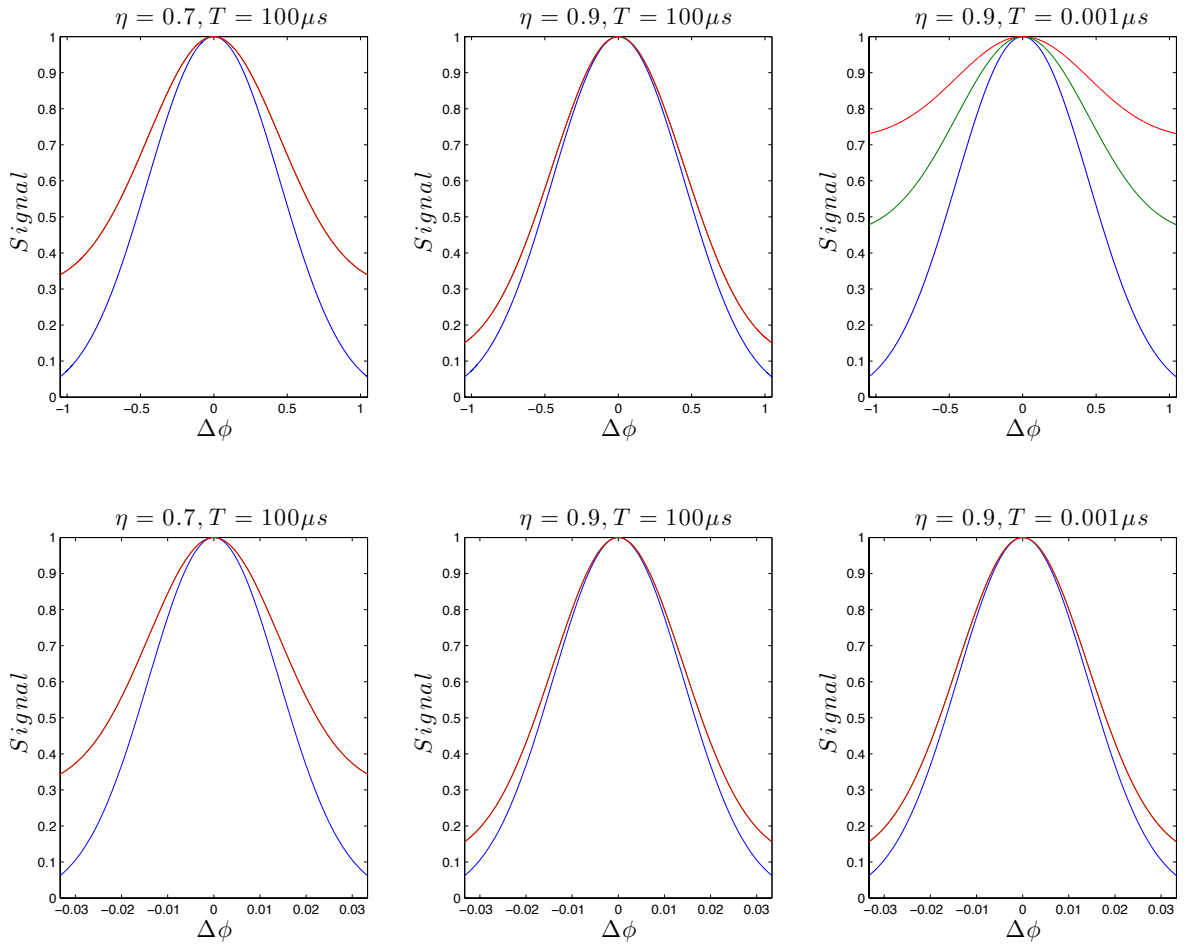

FIG. 8. Plot of ideal signal (blue), the upper bound (red), the lower bound (green) for different detection times, T and detector efficiencies, η for (top) $N = 100$ (bottom) $N = 10,000$.

If we set $\gamma_{sa}T = 1$, the signal depends on η as

$$S_{CSAI} \simeq 1 - \eta(1 - \cos^{2N}(\Delta\phi/2)) \tag{21}$$

for large N and $\mathscr{M} = 1$. Hence, we can calculate the QRF for the CSAI to see how it depends on the detector efficiency, and how it compares to the CRAI. For the CRAI, it is straightforward to show that with $S_{CRAI} = \eta N \cos^2(\Delta\phi/2)$, the quantum mechanical noise in the signal is $\Delta S_{CRAI} = \sqrt{\eta N}\cos(\Delta\phi/2)\sin(\Delta\phi/2)$ and the RVS is $|\partial S_{CRAI}/\partial\Omega_G| = (\eta N/\gamma_{sa})\cos(\Delta\phi/2)\sin(\Delta\phi/2)$, so that the QRF is $\delta\Omega_{G(QM,CRAI)} = \gamma_{sa}/\sqrt{\eta N}$. It is also straightforward to calculate the QRF of the CSAI. the total quantum mechanical noise in the CSAI signal in Eq. 21 is:

$$\Delta S_{QM,CSAI} = \eta\cos^N(\Delta\phi/2)\sqrt{1 - \cos^{2N}(\Delta\phi/2)}, \tag{22}$$

and the RVS is

$$\partial S_{CSAI}/\partial\Omega_G = -(\eta N/\gamma_{sa})\sin(\Delta\phi/2)\cos^{2N-1}(\Delta\phi/2). \tag{23}$$

Thus, the QRF of the CSAI is

$$\delta\Omega_{G(QM,CSAI)} = \left|\frac{\gamma_{sa}}{N\sqrt{\eta}}\frac{\sqrt{1-\cos^{2N}(\mu\Omega_G/2)}}{\cos^{N-1}(\mu\Omega_G/2)\sin(\mu\Omega_G/2)}\right| \tag{24}$$

which approaches $\gamma_{sa}/\sqrt{\eta N}$ as $\Omega_G \to 0$. Assuming that the detector efficiencies of the CSAI and the CRAI can be essentially the same, they do not affect the ratio of the two QRF's.

VI. EFFECT OF COLLECTION EFFICIENCY

We consider next the effect of collection efficiency, β on the CSAI and compare it to that of the CRAI. The signal for both the CSAI and the CRAI, is directly proportional to β. From Eq. 8 and Eq. 11, it is easy to show that

$$\zeta \equiv \frac{\delta\Omega_{G(QM,CSAI)}}{\delta\Omega_{G(QM,CRAI)}} = \left[\frac{1}{\sqrt{N}}\frac{\sqrt{1-\cos^{2N}(\mu\Omega_G/2)}}{\cos^{N-1}(\mu\Omega_G/2)\sin(\mu\Omega_G/2)}\right]\sqrt{\frac{\beta_{CRAI}}{\beta_{CSAI}}}, \tag{25}$$

where $\beta_{CRAI}(\beta_{CSAI})$ is the collection efficiency of the CRAI (CSAI).

As $\Omega_G \to 0$, the quantity in the square bracket in Eq. (25) approaches unity. Therefore, in this limit, ζ, the ratio of the QRF of the CSAI to that of the CRAI, would depend on the ratio of of the collection efficiencies of the detection process. As discussed in the main body of this paper, the coherent stimulated Raman scattering based detection method used for the CSAI process has a collection efficiency that is close to unity, i.e. $\beta_{CSAI} \simeq 1$. In the case of the CRAI, the fluorescence is collected from the spontaneous emission process, which emits photons in a dipolar radiation pattern. The β_{CRAI} can be quantified by analyzing the detection method, for example, of a CRAI that makes use of cold atoms released from a MOT. For a lens placed at a distance of $r = 5$ cm, with a diameter of $d = 2.5$ cm, ignoring the dipolar pattern of radiation for simplicity, and assuming it to be uniform in all directions, this system yields a value of $\beta_{CRAI} \simeq d^2/4r^2 = 1/16$ corresponding to $\zeta \sim 0.25$. In a typical CRAI, various geometric constraints make it difficult to achieve a value of β_{CRAI} much larger than this. In practice, in cases where the total volume occupied by the CRAI has to be constrained in order to meet the user requirements, the value of β_{CRAI} is typically

1%, which would correspond to $\zeta \sim 0.1$. Thus, the near unity collection efficiency of the CSAI can lead to an improvement of the interferometer stability by as much as a factor of 10.

---

[1] M. G. Sagnac, C. R. Acad. Sci. **157**, 708 (1913).

[2] M. O. Scully and J. P. Dowling, Phys. Rev. A 48, 3186 (1993).

[3] G. B. Malykin, Phys. Usp. 43, 1229 (2000).

[4] L. De Broglie, Thesis, University of Paris, Paris, France (1924).

[5] S.-Y. Lan et al., Science 339, 554-557 (2013).

[6] D. B. Hume, C. W. Chou, T. Rosenband, and D. J. Wineland, Phys. Rev. A **80**, 052302 (2009).

[7] R. Sarkar, M. E. Kim, R. Fang, Y. Tu, and S.M. Shahriar, (2014), arXiv:1408.2296.

[8] M. Kasevich and S. Chu, Phys. Rev. Lett. 67, 181-184 (1991).

[9] W. M. Itano, J. C. Bergquist, J. J. Bollinger, J. M. Gilligan, D. J. Heinzen, F. L. Moore, M. G. Raizen, and D. J. Wineland, Phys. Rev. A 47, 3554-3570 (1993).

[10] M. O. Scully, E. S. Fry, C. H. Raymond Ooi, and K. Wódkiewicz, Phys. Rev. Lett. 96, 010501 (2006).

[11] L. M. Duan, M. D. Lukin, J. I. Cirac, and P. Zoller, Nature (London) 414, 413 (2001).

[12] C. W. Gardiner and P. Zoller, Quantum Noise (Springer-Verlag, Berlin, 1999).